Huang and Zhu *Anthropocene Coasts* (2023) 6:3
https://doi.org/10.1007/s44218-023-00019-5

Anthropocene Coasts

RESEARCH ARTICLE

Open Access

Suspended sediment dynamics and influencing factors during typhoons in Hangzhou Bay, China

Ju Huang and Jianrong Zhu*

Abstract

Hangzhou Bay is located in China on the south side of the Changjiang Estuary and is vulnerable to extreme weather, such as typhoons in the summer and autumn. In this study, a three dimensional suspended sediment numerical model was developed that considers the dynamic factors of advection, mixing, wave, and sediment-induced stratification to simulate and analyze the effect of typhoons on water and sediment transport in Hangzhou Bay. The model validations show that the model can sufficiently reproduce the variability of the suspended sediment concentration (SSC) during typhoon conditions. The simulation results show that the high SSC in the bottom layer was mainly distributed in the leading edge of the south coast, and generally exceeded 10 kg·m^{-3}. During typhoons, the water and suspended sediment transport in Hangzhou Bay presented a pattern of "north-landward and south-seaward" circulation, which promoted the convergence of suspended sediment in the center part of the bay. During Typhoon Rumbia in 2018, the water and sediment flux across the section from Nanhui Cape to Qiqu Archipelago (NQ section) increased by 18.13% and 265.75%, respectively, compared with those before the typhoon. The wave-induced bottom shear stress during typhoons has a very significant impact on the bottom SSC. The sensitivity experiments show that the wave-induced bottom shear stress greatly promotes the sediment resuspension during typhoons, which indirectly makes the sediment-induced stratification stronger than the direct effect of waves on the vertical mixing. The strong winds brought by typhoons mainly enhanced the vertical mixing, which has a stronger effect on surface SSC than waves. The suppression of vertical mixing by sediment-induced stratification during typhoons should not be ignored, especially for high turbidity coastal waters, such as Hangzhou Bay.

Keywords Sediment transport, Typhoons, Wave, Stratification, Hangzhou Bay, Numerical model

1 Introduction

Suspended sediments are carriers of nutrients, organic matter, and pollutants that impede light transmission, photosynthesis, and primary productivity and affect the marine environment and ecological processes (Fang et al. 2016; Li et al. 2016a; Zhao et al. 2018). Though there are numerous factors, typhoons are undoubtedly an important mechanism that drives drastic changes in suspended sediment concentration (SSC) in bays. The East China Sea is affected by four typhoons every year on average (Lu et al. 2018).Very high waves are generated during typhoons, these waves propagate into nearshore areas and induce phenomena such as wave reflection, refraction, and fragmentation. In recent years, the intensity and frequency of extreme events, such as typhoons, have increased, and the impact of typhoons on sediment resuspension and redistribution in coastal waters has gradually attracted increasing attention from oceanographers (Bian et al. 2010; Gong and Shen 2009; Lu et al. 2018; Palinkas et al. 2014; Xie et al. 2018). Analyzing

*Correspondence:
Jianrong Zhu
jrzhu@sklec.ecnu.edu.cn
State Key Laboratory of Estuarine and Coastal Research, East China Normal University, Shanghai 200241, China

how waves influence the sediment transport and deposition/resuspension processes in coastal bays is of critical importance to studies of coastal geomorphology or for research exploring the ecological effects of typhoons (Liu et al. 2022; Zhang et al. 2021).

In recent years, the supply of fluvial sediments to estuarine and coastal systems has been significantly reduced due to upstream dams (Syvitski et al. 2009, 2005). With the reduction of sediment entering the sea, tidal currents and waves play an important role in maintaining the SSC in coastal waters. For example, Huang et al. (2021) concluded that the main reason for the slow decline of SSC in the Changjiang Estuary and its adjacent waters is related to wave and tide-induced sediment resuspension. Luo et al. (2017) found that the bottom sediment resuspension was mainly caused by tide-induced shear stress and diffused to the surface layer by vertical mixing in winter. The waves increase the bottom shear stress through wave-current interaction, thus effectively promoting sediment resuspension (Hsu et al. 2006; Xu and You 2017). For example, Xu and You (2017) studied the effects of waves on sediment resuspension in the Oujiang Estuary, China. Zhang et al. (2021) studied wave effects on water and sediment transport in the Pearl River Estuary, China, and the results showed that the wave effects were strongest in winter and enhanced the sediment deposition in the western shoal of the Pearl River Estuary. The effect of waves on SSC is more significant during typhoons. Shen et al. (2018) and Ren et al. (2021) concluded that waves during typhoons greatly contributed to sediment resuspension in the Changjiang Estuary. Brand et al. (2010) concluded that the wave effects increased SSC from 30 mg·L^{-1} during calm periods to more than 100 mg·L^{-1} during turbulent periods at the shoals in the southern portion of San Francisco Bay, USA. In addition, waves can change the vertical stratification of the estuary and affect the distribution of suspended sediment and its transport direction (Green and Coco 2014).

Hangzhou Bay is located on the south side of the Changjiang Estuary (Fig. 1), connects to the Qiantang River in the west, and is characterized by a large irregular and semidiurnal tide, strong flow, and high SSC. Morphologically, Hangzhou Bay is an east–west oriented trumpet shaped bay. The bay has one of the highest SSC in the world. With the development of numerical models, some researchers have used numerical models to carry out SSC research in Hangzhou Bay. Xie et al. (2009) developed a two-dimensional suspended sediment numerical model in Hangzhou Bay to obtain sediment transport directions. Du et al.

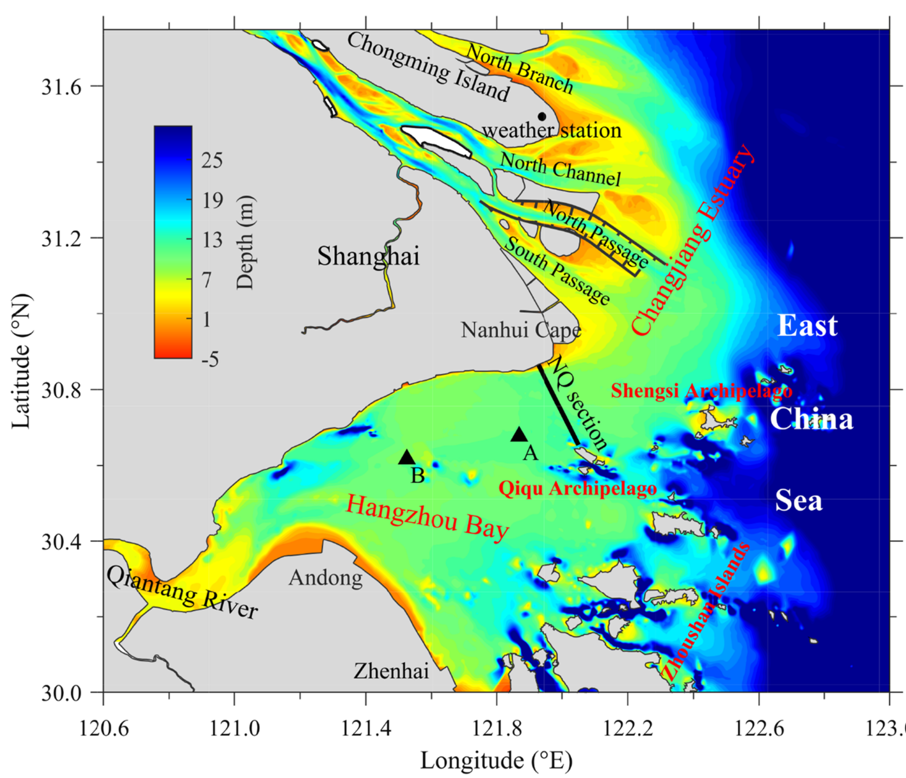

Fig. 1 Map of Hangzhou Bay and Changjiang Estuary. Black triangle: the anchored ship stations; thick black line: the section from Nanhui Cape to Qiqu Archipelago; black dot: Chongming weather station

(2010) used a three-dimensional suspended sediment model to analyze the temporal variation in SSC during the neap-spring tidal cycle in Hangzhou Bay. Xie et al. (2013) used the Delft3D to find that sediment transport in Hangzhou Bay was affected by tidal asymmetry. Because the bay mouth is occupied by Zhoushan Islands, it is not easy for waves from the outer sea to enter the bay. The waves in Hangzhou Bay are weak under normal weather conditions, with an annually averaged wave height of 0.2–0.5 m (Xie et al. 2013). However, Hangzhou Bay has large waves during typhoons and is affected by typhoons almost every year. Li et al. (2022a) concluded that the SSC in Hangzhou Bay was most affected by waves during Typhoon Chanhom based on FVCOM. Li et al. (2022b) concluded that the combined wave-current bottom stress was the primary wave-current interaction that changed sediment resuspension and increased SSC. Due to the difficulty of actual observation data during typhoons, research on the SSC characteristics in Hangzhou Bay during typhoon conditions is still relatively lacking.

Based on the improved ECOM-si (Estuary, Coast, and Ocean Model with semi-implicit), a high resolution three dimensional numerical model of suspended sediment in Hangzhou Bay is developed. The model takes into consideration advection, diffusion, settlement, sediment flocculation, waves, and sediment-induced stratification, to simulate the sediment transport in Hangzhou Bay under typhoon conditions. The model description and validation are presented in Sect. 2. In Sect. 3, the water and suspended sediment transport process in Hangzhou Bay during typhoons are analyzed. The sensitivity analysis for the different factors is presented in Sect. 4. Finally, the conclusion is presented in Sect. 5.

2 Materials and methods

2.1 Observations

The State Key Laboratory of Estuarine and Coastal Research, East China Normal University, conducted continuous field observations in Hangzhou Bay from August 5 to 20, 2018. Two marine research ships collected simultaneously observations at site A and site B (Fig. 1). Tripod-mounted observation systems were placed on the seafloor at each site. The instruments mounted in each tripod were positioned 0.2 m above the bottom. A 600 kHz acoustic Doppler current profiler (ADCP, RD Instruments) was used to measure the vertical current profile; an optical backscatter sensor (OBS, D&A Instrument Company) was used to measure salinity, temperature, and turbidity; a Sea-Bird SBE37 CTD was used to measure temperature and salinity; and an electromagnetic current meter (Alec, Electronics, Tokyo) was used to measure the near-bottom current inaccessible by the ADCP. The ADCP worked in upward-looking mode at a vertical resolution of 0.25 m and ensembles of 2 min at a 1-s ping interval. A diagram of the instrument positions is shown in Fig. 2. Water samples were taken at the sites and brought back to the laboratory for SSC measurements to determine the relationship between OBS turbidity and SSC. Surface data could not be obtained during typhoons Yagi and Rumbia, which impacted the site in 2018.

At 23:00 on August 12, 2018, Typhoon Yagi made landfall on the coast of Zhejiang, China, with a maximum

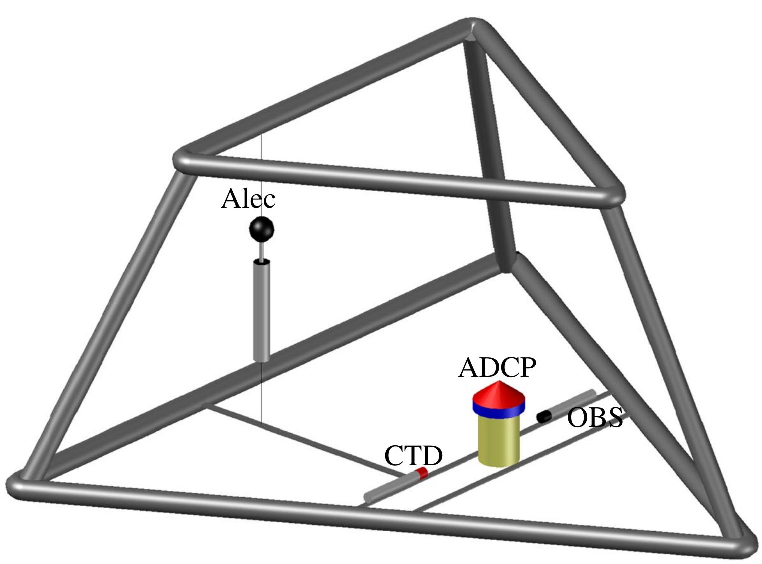

Fig. 2 Tripod observation system and positions of the instruments

wind speed of 28 m/s; at 4:00 on August 17, 2018, Typhoon Rumbia directly passed through Hangzhou Bay and made landfall off the southern coast of Shanghai with a maximum wind speed of 23 m/s (Fig. 3). The tripod observation systems at sites A and B continuously recorded the variations in benthic hydrodynamics and SSC during the typhoon period from August 12 to August 18, 2018. The weather station located on Chongming Island recorded wind speed changes during typhoons. Since Chongming Island is far from the center of Typhoon Yagi, its maximum wind speed was approximately 13 m/s, while the center of Typhoon Rumbia was close to Chongming Island, and its maximum wind speed was approximately 20 m/s (Fig. 4). The impact of Typhoon Rumbia on Hangzhou Bay is more significant than that of Typhoon Yagi. The ERA5 (ECMWF Reanalysis v5) wind field data from the ECMWF (European Centre for Medium-Range Weather Forecast, https://cds.climate.copernicus.eu/cdsapp#!/dataset/reanalysis-era5-single-levels?tab=overview) are consistent with the actual wind speed and direction measured by the weather station and can accurately reproduce the wind speed variability during typhoons (Fig. 4). Figure 5 shows the wind field distribution at 03:00 on August 13, 2018 (Typhoon Yagi) and at 00:00 on August 17, 2018 (Typhoon Rumbia). Due to the influence of Typhoon Yagi, the wind direction in Hangzhou Bay was mainly southeast (Fig. 5a), and due to Typhoon Rumbia, the wind field in Hangzhou Bay was mainly cyclonic (Fig. 5b).

2.2 Numerical model setup

The improved three dimensional ECOM-si includes a hydrodynamic model, a sediment module, and the SWAN (Simulating Waves Nearshore) model, which provides wave parameters for the hydrodynamic model and sediment module. The hydrodynamic model originated from the POM (Princeton Ocean Model) developed by Princeton University (Blumberg and Mellor 1987). The model uses the "Arakawa C" grid configuration variables (Arakawa and Lamb 1977). A nonorthogonal curve grid was used in the horizontal direction (Chen et al. 2004), and the sigma coordinate was adopted in the vertical direction. The level 2.5 turbulence closure model by Mellor and Yamada (1982) was used to calculate the vertical mixing coefficients, and the parameter formula of the stability function was from Kantha and Clayson (1994), while the parameterization scheme of Smagorinsky (1963) was used to calculate the horizontal mixing coefficients. A wet/dry scheme was included to describe the intertidal flat with a critical depth of 0.2 m. To reduce the numerical dissipation and improve the computational accuracy in the material transport process, Wu and Zhu (2010) developed the high order spatial interpolation at the middle temporal level coupled with a TVD limiter

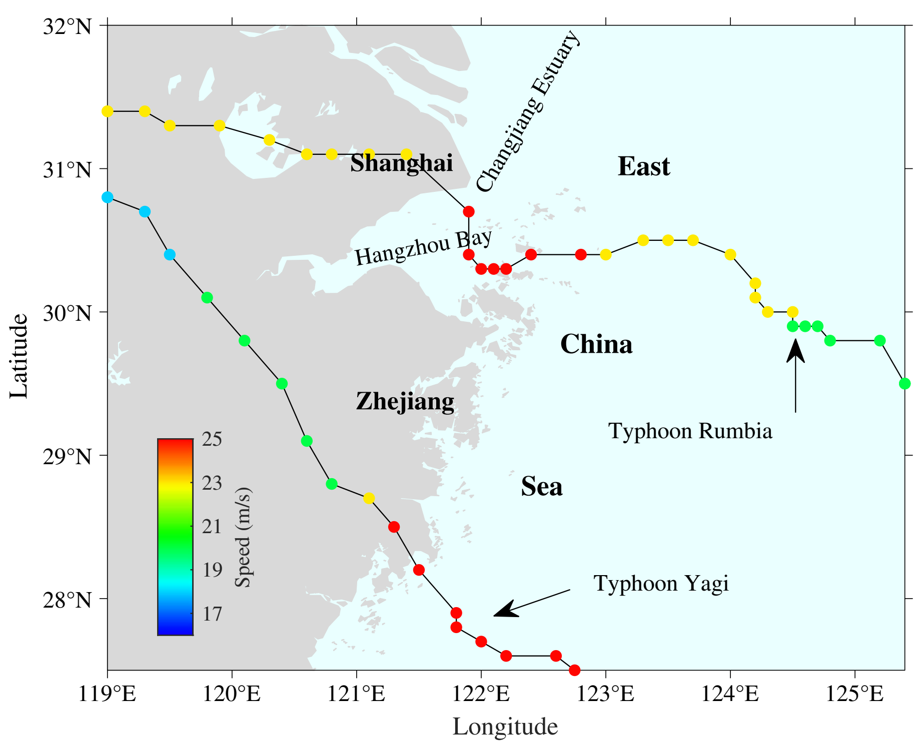

Fig. 3 Paths of Typhoon Yagi and Typhoon Rumbia in 2018 before and after landfall

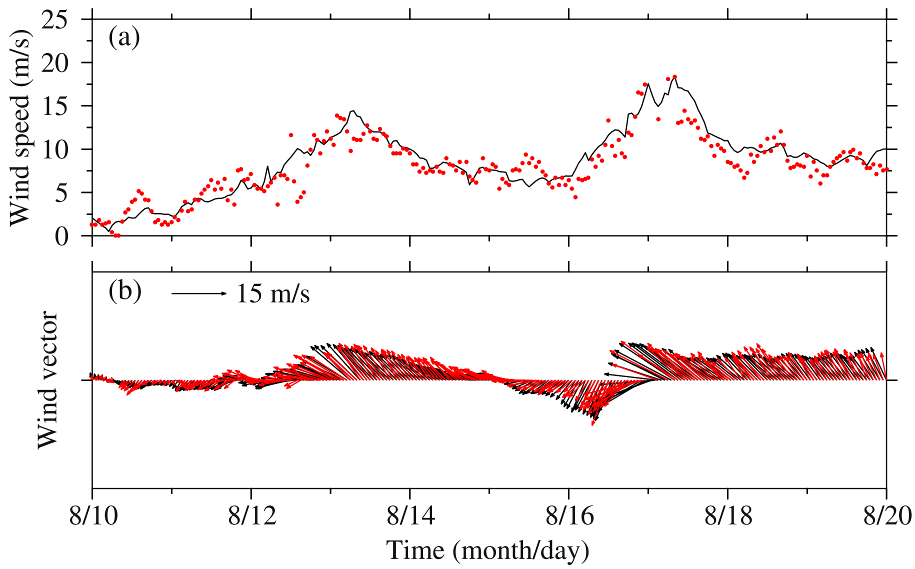

Fig. 4 Temporal variations in wind speed (**a**) and wind vector (**b**) at Chongming weather station. Red: observed data; black: ERA5 data

to solve the advection term in the material transport equation. The barotropic pressure gradient force in the momentum equation was solved by an implicit method, and the continuous equation was solved by the semi-implicit method of Casulli and Cattani (1994).

The model domain covered all of the Changjiang Estuary and Hangzhou Bay and adjacent seas from 117.5° E to 125° E longitude and 27.9° N to 33.7° N latitude (Fig. 6a). The model grid consisted of 396 × 522 cells in the horizontal dimension. Fifteen sigma levels were set in the vertical direction with five logarithmically distributed layers near the bottom ($\sigma = -0.929, -0.964, -0.982, -0.991, -1.0$) to distinguish the effect of high bottom SSC on the bottom friction drag coefficient, and 10 layers were established in the remaining layers ($\sigma = 0, -0.1, -0.2, -0.3, -0.4, -0.5, -0.6, -0.7, -0.79, -0.87$). The grid resolution ranges between 200 m at the top of the bay, approximately 600 m in the central part, and is 2 ~ 10 km near the open sea boundary (Fig. 6b).

The open sea boundary condition was specified by the tide and residual water level. The tidal signal was composed of 16 astronomical constituents, M_2, S_2, N_2, K_2, K_1, O_1, P_1, Q_1, MU_2, NU_2, T_2, L_2, $2N_2$, J_1, M_1, and OO_1, which were derived from the NaoTide dataset (http://www.miz.nao.ac.jp/). The residual water level and initial salinity field were derived from the results simulated by a large domain model encompassing the Bohai Sea, Yellow Sea, and East China Sea (Wu et al. 2011). The river boundary was driven by the river discharge at the Datong hydrologic station (Changjiang Water Resources Commission) for the Changjiang River and at the Fuchunjiang hydroelectric power station for the Qiantang River. Wind data were adopted from the ERA5 dataset, with a temporal resolution of 6 h and a spatial resolution of 0.25° × 0.25°.

For a detailed introduction to the sediment module, please refer to the author's other article (Huang et al. 2022). In the model, the sediment in the water body is considered cohesive fine grained sediment. The role of waves in sediment resuspension cannot be ignored, especially during typhoon conditions. The improved model algorithm calculates the bottom wave orbit velocity with sea surface wave parameters to obtain the bottom shear stress generated by the waves. This algorithm needs to use the significant wave height, average wave direction, and significant wave period on the sea surface. The bottom shear stress under the influence of wave-current interaction is given by (Grant and Madsen 1979):

$$\begin{aligned}\tau &= |\tau_w + \tau_c| = \sqrt{(\tau_w + \tau_c|\cos\varphi|)^2 + (\tau_c\sin\varphi)^2} \\ &= \tau_w\sqrt{1 + 2\frac{\tau_c}{\tau_w}|\cos\varphi| + \left(\frac{\tau_c}{\tau_w}\right)^2}\end{aligned} \tag{1}$$

where τ is the bottom shear stress considering waves and currents; τ_w is the maximum wave-induced bottom shear stress; τ_c is the tidal-induced bottom shear stress; ϕ is the angle between wave propagation and the current direction. τ_c and τ_w can be calculated by:

$$\tau_c = \rho C_d U^2 \tag{2}$$

$$\tau_w = \frac{\rho f_w}{2} U_w^2 \tag{3}$$

where ρ is the actual density of seawater with the suspended sediment; U is the bottom current velocity; C_d is

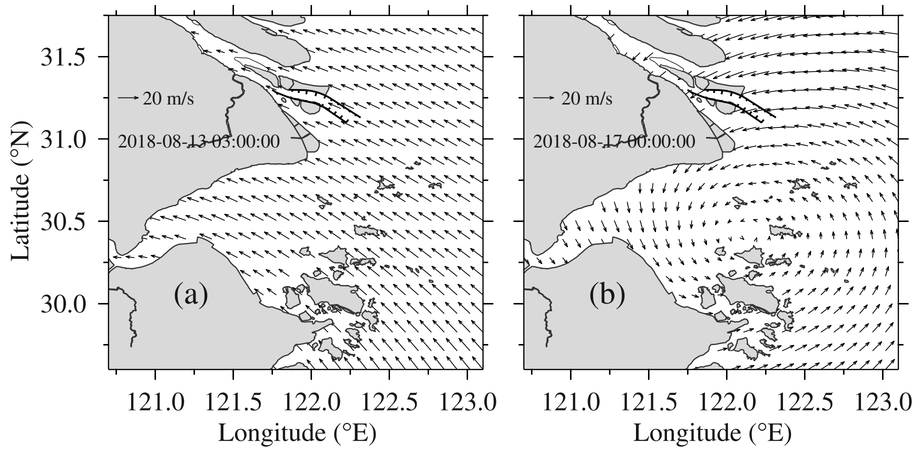

Fig. 5 Wind field distribution during Typhoon Yagi (**a**) and Typhoon Rumbia (**b**)

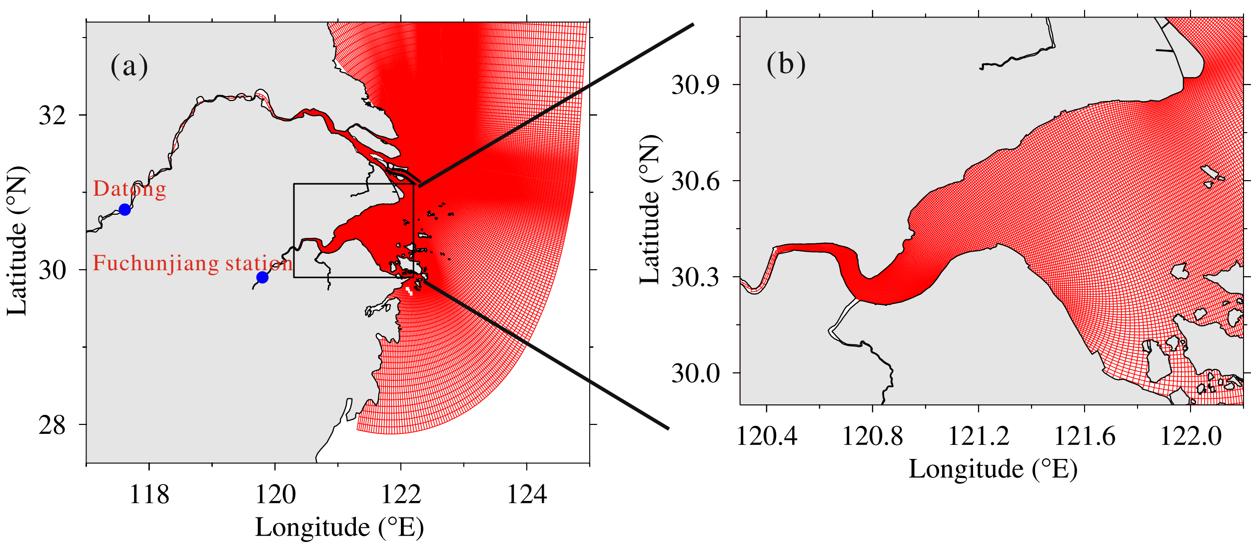

Fig. 6 Numerical model domain and grid (**a**) and an enlarged view of the model grid in Hangzhou Bay (**b**)

the bottom drag coefficient; f_w is the wave fiction factor; and U_w is the near-bed wave orbital velocity. A detailed calculation procedure can be found in Wiberg and Sherwood (2008). Waves affect not only the bottom shear stress but also the vertical mixing coefficient (Mellor and Blumberg 2004; Terray et al. 1999). Based on the level 2.5 turbulence closure module, Mellor and Blumberg (2004) considered the effect of waves breaking on the sea boundary layer. The sea surface boundary conditions are:

$$K_q \frac{\partial q^2}{\partial z} = 2\alpha_{CB} u_\tau^3, z = 0 \quad (4)$$

where q^2 is the turbulence kinetic energy;u_τ is the water side friction velocity;α_{CB} is a parameter related to the waves, with the following equation:

$$\alpha_{CB} = 15\left(\frac{C_p}{u_*}\right) \exp\left[-\left(\frac{0.04C_p}{u_*}\right)^4\right] \quad (5)$$

where C_p/u_* is the wave age;C_p is the phase speed of waves at the dominant frequency; u_* is the air side friction velocity; and $u_* = 30u_\tau$. When the effect of waves is not considered, $q^2 = {B_1}^{2/3}u_\tau^2$ at z=0, $B_1 = 16.6$. When the effect of waves is considered, $q^2 = (15.8\alpha_{CB})^{2/3}u_\tau^2$ at z=0. From measured wave heights and near-surface dissipation data, Terray et al. (1999) used the turbulence closure module to find the best fit between the turbulent mixing length (l) and the measured data.

$$l = \max(\kappa z_w, l_z), z_w = 0.85H_s \quad (6)$$

where H_s is the significant wave height; $l_z = \kappa z$; $\kappa = 0.4$ is the von Karman constant. When the effect of waves is not considered, $z_w = 0.K_m = qlS_M$ is the vertical eddy viscosity; $K_h = qlS_H$ is the vertical eddy diffusivity, where S_M and S_H are the stability function, please refer to Mellor and Yamada (1982).

The SWAN model (Booij et al. 1999) adopted an orthogonal mesh that covered the calculation range of the ECOM-si, with a spatial resolution of 2' × 2' and a time step of 30 min. The SWAN model outputted the significant wave height, significant wave period, and wave direction every 3 h, and these parameters were interpolated to each time step in the sediment module to calculate the bottom shear stress and vertical mixing coefficient under wave-current interactions. The wave parameters output from the SWAN model has been validated in related papers by our research group (Luo et al. 2017).

2.3 Model validation

The ECOM-si has been extensively validated in terms of water level, current speed and direction, salinity, and SSC (Chen et al. 2019; Luo et al. 2017; Lyu and Zhu 2018; Qiu and Zhu 2013; Wu and Zhu 2010; Zhu et al. 2015). This study will further validate the model in Hangzhou Bay. The following three skill assessments were used to quantify the validation of the model: correlation coefficient (CC), root mean square error (RMSE), and skill score (SS) (Murphy 1988; Warner et al. 2005; Willmott 1981):

$$CC = \frac{\sum \left(X_{mod} - \overline{X_{mod}}\right)\left(X_{obs} - \overline{X_{obs}}\right)}{\left[\sum \left(X_{mod} - \overline{X_{mod}}\right)^2 \sum \left(X_{obs} - \overline{X_{obs}}\right)^2\right]^{\frac{1}{2}}} \quad (7)$$

$$SS = 1 - \frac{\sum \left(X_{mod} - X_{obs}\right)^2}{\sum \left(\left|X_{mod} - \overline{X_{mod}}\right| + \left|X_{obs} - \overline{X_{obs}}\right|\right)^2} \quad (8)$$

$$RMSE = \sqrt{\frac{\sum \left(X_{mod} - X_{obs}\right)^2}{N}} \quad (9)$$

where X is the variable and $\bar{X}$ is the time-averaged value. The performance levels of the modeled results and observed results were evaluated by SS where SS > 0.65 is considered excellent, 0.65–0.5 is very good, 0.5–0.2 is good, and SS < 0.2 is considered poor.

The modeled current velocity, current direction, salinity, and SSC were validated with observation data during neap tide and spring tide at site A and site B in Hangzhou Bay in August 2018; see Huang et al. (2022). This study used data that included typhoon periods to validate the model. We downloaded the real-time river discharge data for the Datong hydrological station and Fuchunjiang hydropower station, as well as the real-time wind field data from ERA5 to drive the model. The model was cold started on 1 July 2018 and ran for 62 days. The comparison between the simulated water level and the measured data from August 6 to 20, 2018, is shown in Fig. 7. Hangzhou Bay is famous for its strong tides. In terms of tidal nature, the tides outside the mouth of the bay are regular semidiurnal tides and inside the bay mouth, they are irregular semidiurnal tides. After August 12, Hangzhou Bay was impacted by Typhoon Yagi and Typhoon Rumbia. Regardless of whether it was normal or typhoon conditions, the simulated water level was consistent with the measured value, and both the SS and CC exceeded 0.95 (Table 1), indicating that the model can successfully simulate the temporal variation in water level.

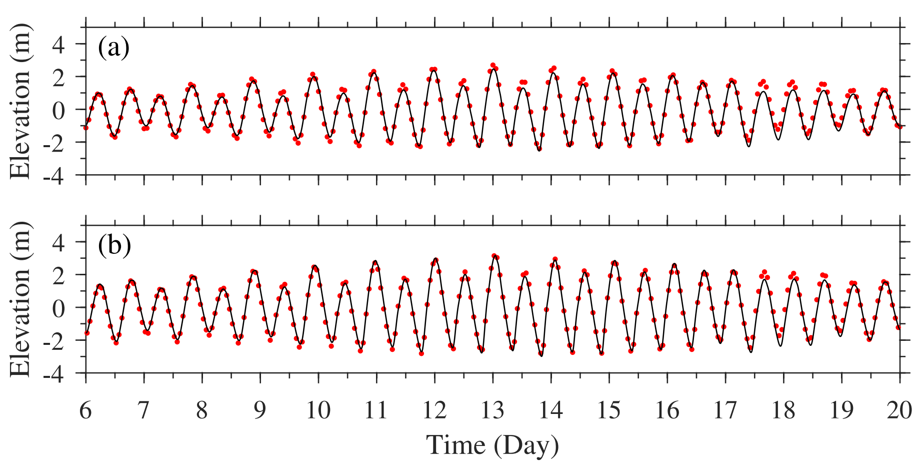

Fig. 7 Comparison of the simulated water level (black line) and measured data (red dot) at site A (**a**) and site B (**b**) in Hangzhou Bay from August 6 to 20, 2018

Table 1 Correlation coefficients (CC), root mean square error (RMSE), and skill scores (SS) for comparison of the simulated and observed data at the measuring stations

Skill assessment	Site A			Site B		
	CC	RMSE	SS	CC	RMSE	SS
Water level	0.99	0.25 m	0.99	0.99	0.24 m	0.99
Surface velocity	0.93	0.22 $m\cdot s^{-1}$	0.96	0.95	0.17 $m\cdot s^{-1}$	0.98
Bottom velocity	0.90	0.14 $m\cdot s^{-1}$	0.95	0.85	0.18 $m\cdot s^{-1}$	0.89
Bottom SSC	0.70	1.09 $kg\cdot m^{-3}$	0.83	0.50	1.07 $kg\cdot m^{-3}$	0.71

The simulated current velocity, direction, and SSC are compared with the observed data during typhoons in Fig. 8. Due to the effect of bottom friction, the current velocity in the bottom layer was smaller than that in the surface layer. The average SSC in the bottom layer at site A was 2.78 $kg\cdot m^{-3}$, and the average SSC in the bottom layer at site B was 2.85 $kg\cdot m^{-3}$ during typhoons. The CC, RMSE, and SS of the simulated data and the observation data are shown in Table 1. Note that the SS of the SSC is above 0.7. The model can successfully reproduce the variability in the current velocity, direction, and SSC during typhoon conditions, and can be used to study the hydrodynamic and SSC transport process in Hangzhou Bay.

3 Results

To describe the transport of water and suspended sediment, the residual unit width water flux (RUWF) and the residual unit width sediment flux (RUSF) were used to reflect the transport of water and suspended sediment, which is defined as:

$$\text{RUWF} = \frac{1}{T}\int_0^T \int_{h_1}^{h_2} \vec{V}\, dzdt \tag{10}$$

$$\text{RUSF} = \frac{1}{T}\int_0^T \int_{h_1}^{h_2} \vec{V}\cdot C\cdot\, dzdt \tag{11}$$

where $\overline{V}$ is the instantaneous horizontal velocity vector; h_1 and h_2 are the depths at the lower and upper boundaries of a certain layer, respectively; T is one or more complete cycles; C is the SSC; and the unit width is 1 m. In this study, three semidiurnal tidal cycles were used as an averaging time window to remove the semidiurnal and diurnal tidal signals. The thickness of the surface and bottom layers was one-tenth of the total water depth over the tidal cycle. This method has been used in many studies (Chen et al. 2019; Li et al. 2016b; Lyu and Zhu 2018; Zhu et al. 2015). For the convenience of research, this paper chooses Typhoon Rumbia that directly through Hangzhou Bay as a case study, and its impact on Hangzhou Bay is more significant than that of Typhoon Yagi.

3.1 SSC

The distribution of the bottom SSC at four moments of the tidal cycle in Hangzhou Bay during Typhoon Rumbia is shown in Fig. 9. At the maximum flood, the high SSC in the bottom layer was mainly distributed in the southeastern part of Hangzhou Bay; at the flood slack, the high SSC in the bottom layer was mainly distributed in the south shore tidal flats and southeastern part of the bay, generally exceeding 10 $kg\cdot m^{-3}$. At the maximum ebb, the high SSC in the bottom layer was mainly located on the south coast and in the northern part of the bay; at the ebb slack, the high SSC in the bottom layer was mainly distributed in the leading edge of the south coast, and generally exceeded 10 $kg\cdot m^{-3}$. Through the comparison of the SSC distribution at four moments, it can be found that when the current velocity was high during the typhoon, the water mixing was stronger, and the bottom SSC was generally lower; when the current velocity was low, the southeastern part of Hangzhou Bay near the south coast was the main area for sediment fall siltation, which was also the high value area for sediment.

3.2 Water flux and sediment flux

The distribution of RUWF and RUSF during Typhoon Rumbia is shown in Fig. 10. Typhoon Rumbia occurred during moderate tide and landed directly in Hangzhou Bay. The characteristics of surface RUWF (Fig. 10a) and RUSF (Fig. 10b) during the typhoon were mainly related to the shape of the local wind (Fig. 5b), with surface sediment transport in Hangzhou Bay extending all the way to the top of the bay. And surface water and suspended sediment entered from the north coast in Hangzhou Bay and was then transported to the sea from the south coast, forming a counterclockwise circulation pattern in the bay. The bottom RUWF (Fig. 10c) transported a longer distance along the north coast than the bottom RUSF (Fig. 10d), but they all converged in the central part of Hangzhou Bay. The RUWF (Fig. 10e) and RUSF (Fig. 10f) in the whole layer showed the pattern of "north-landward and south-seaward" in Hangzhou Bay, and the water and sediment mainly came from the Changjiang Estuary, which was

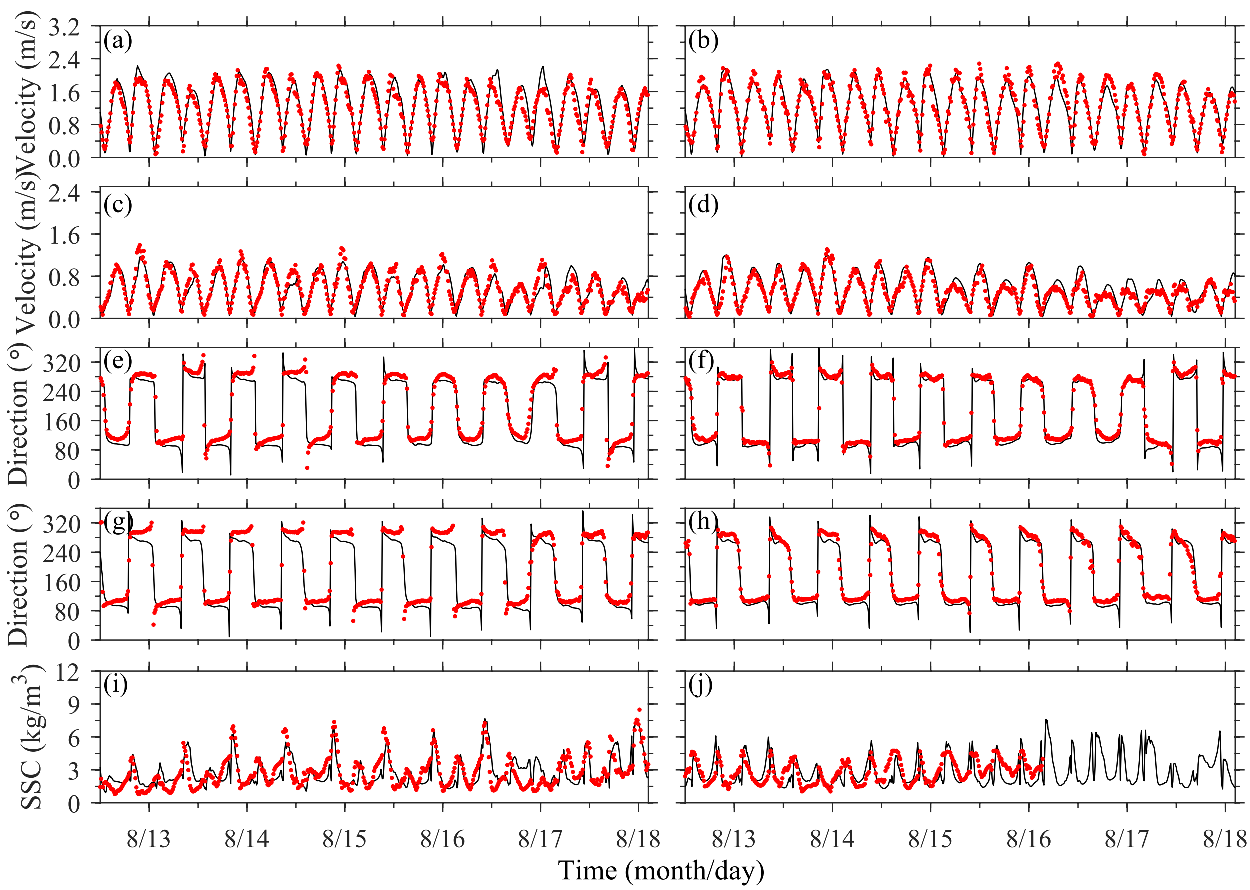

Fig. 8 Comparisons between the observed data (red dots) and simulated results (black line) at study site A (left panel) and site B (right panel). **a**, **b** surface velocity; **c**, **d** bottom velocity; **e**, **f** surface direction; **g**, **h** bottom direction; **i**, **j** bottom SSC

similar to the distribution of RUWF and RUSF during the spring tide under climatic conditions (Huang et al. 2022). Although Typhoon Rumbia occurred during moderate tide, the water and suspended sediment transport volume in the whole layer were significantly greater than those during the climatological spring tide, while the surface water and suspended sediment transport were mainly determined by the wind field of the typhoon.

The net transect water flux (NTWF) and the net transect sediment flux (NTSF) across a section are calculated using the following equations:

$$\mathrm{NTWF} = \int_0^T \int_{-H}^{\zeta} \int_0^L \overrightarrow{V_n} dldzdt \tag{12}$$

$$\mathrm{NTSF} = \int_0^T \int_{-H}^{\zeta} \int_0^L C\overrightarrow{V_n} dldzdt \tag{13}$$

where ζ is the water level; L is the width of the transect; C is the SSC; $\overrightarrow{V_n}$ is the velocity component normal to the transect; T is three semidiurnal tidal cycles (~ 37 h).

The water and sediment flux across the NQ section before and during the typhoon are shown in Table 2. During Typhoon Rumbia, the NTWF and NTSF across the NQ section increased by 18.13% and 265.75%, respectively, compared with those before the typhoon. It is worth noting that the sediment flux increased more significantly than the water flux, indicating that the typhoon greatly promoted sediment resuspension. Typhoons such as Typhoon Rumbia, which made direct landfall in Hangzhou Bay, can promote more suspended sediment to enter Hangzhou Bay from the mouth of the Changjiang Estuary, which played an important role in the sediment exchange between the Changjiang Estuary and Hangzhou Bay.

4 Discussion

To discuss the effects of sediment-induced stratification, waves, and winds on suspended sediment during typhoons, three numerical sensitivity experiments were

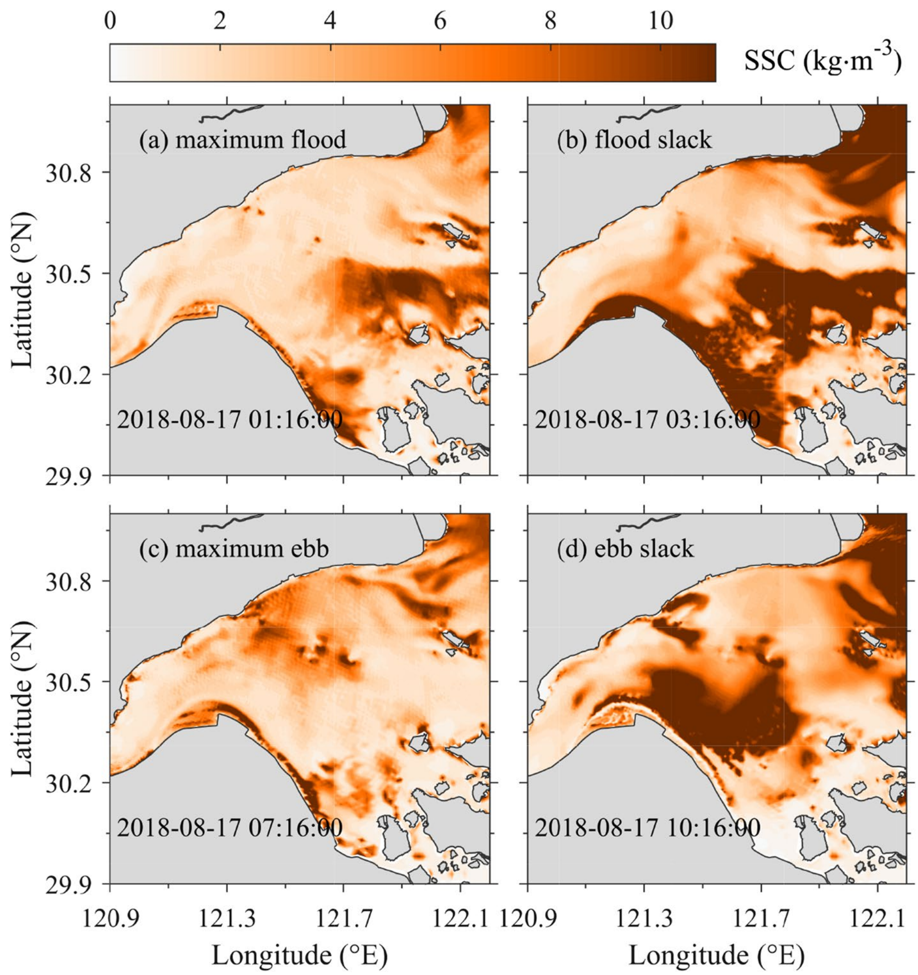

Fig. 9 Modeled bottom SSC at the maximum flood (**a**), flood slack (**b**), maximum ebb (**c**) and maximum ebb (**d**) during Typhoon Rumbia

set up in this study. Exp 1 was without sediment-induced stratification, Exp 2 was without waves, and Exp 3 was without winds. The other dynamic factors were the same as the numerical model settings in Sect. 3, which was called the control experiment (Exp 0).

4.1 Effect of sediment-induced stratification

In high turbidity estuaries, sediment-induced stratification plays an important role in the trapping of bottom sediment (Huang et al. 2022; Zhu et al. 2021). Compared with other estuaries worldwide, the water in Hangzhou Bay is characterized by high turbidity. The formula for the contribution of sediment to density is as follows (Winterwerp 2001):

$$\rho = \rho_w + \left(1 - \frac{\rho_w}{\rho_s}\right)C \tag{14}$$

where ρ_w is the density of seawater without sediment, ρ_s is the density of suspended sediment, and ρ is the actual density of seawater with SSC.

The comparison results of Exp 0 and Exp 1 at sites A and B during the typhoon are shown in Fig. 11. After considering sediment-induced stratification, the simulated surface SSC at sites A and B decreased by 50.8% and 58.6%, respectively; the vertical eddy diffusivity (K_h) decreased by 41.0% and 36.0%, respectively, and the simulated bottom SSC decreased by 27.8% and 37.5%, respectively. The results show that the simulated SSC was much more consistent with the observed values after considering the sediment-induced stratification.

The gradient Richardson number (R_i) is often used to estimate the relative strength of stratification and mixing in the water column (Galperin et al. 2007; Grant and Madsen 1986; Richardson 1920) and can be expressed as:

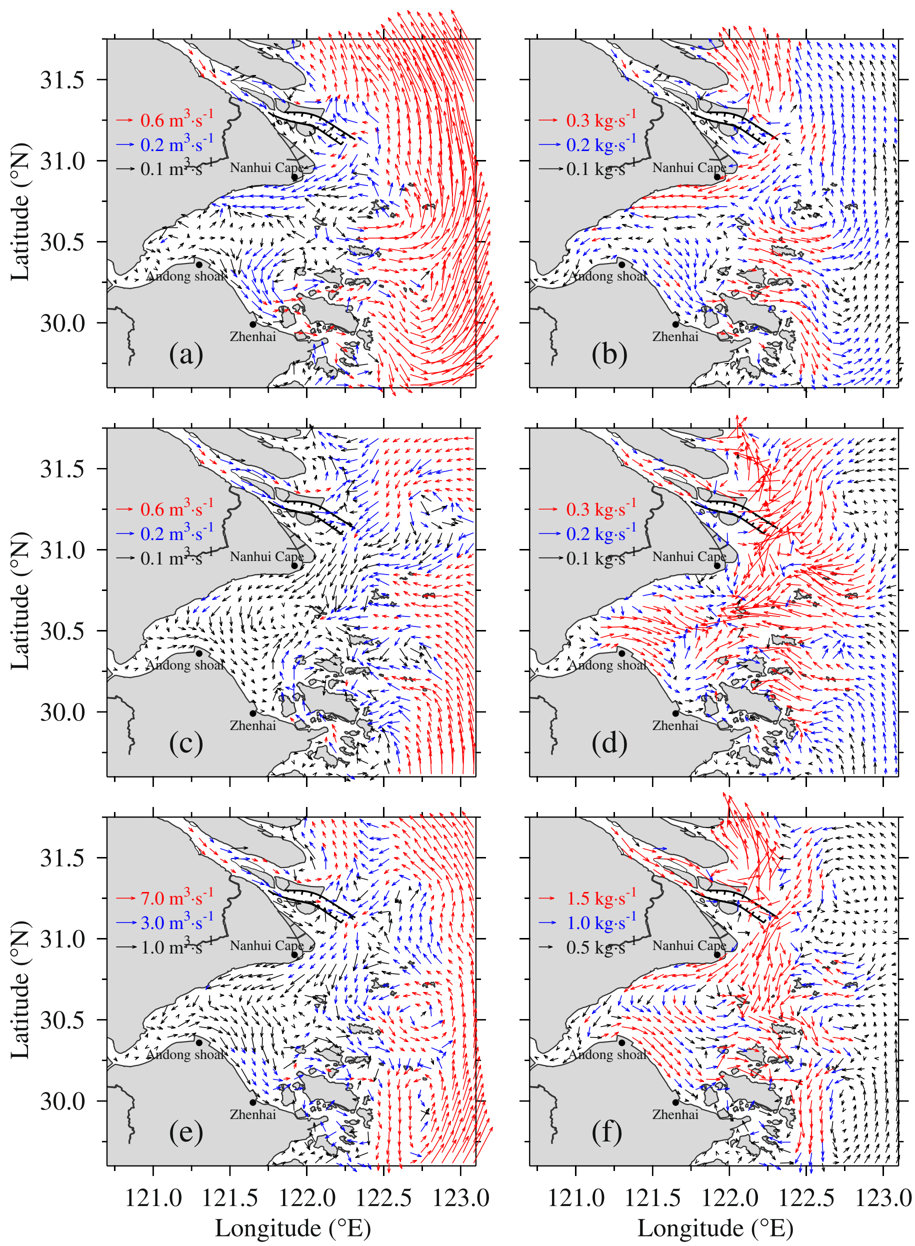

Fig. 10 The distributions of RUWF (left panel) and RUSF (right panel) in the surface layer (**a**, **b**), bottom layer (**c**, **d**), and whole layer (**e**, **f**) during Typhoon Rumbia

Table 2 NTWF and NTSF across the NQ section. Negative values indicate sediment flow into Hangzhou Bay, and positive values indicate sediment flow into the Changjiang Estuary

Flux type	Before Typhoon Rumbia	Typhoon Rumbia	Increasing rate (%)
NTWF (10^9 m^3)	-1.93	− 2.28	18.13
NTSF (10^9 kg)	-1.46	− 5.34	265.75

$$R_i = \frac{-\frac{g}{\rho_0}\frac{\partial \rho}{\partial z}}{(\partial V/\partial z)^2} \tag{15}$$

where ρ is density; V is the vector horizontal velocity; g is the acceleration of gravity; ρ_0 is the reference density; z is the depth. Miles (1961) suggested that R_i has a critical value of 0.25, above which stable stratification tends to occur, while below this value, stratification tends to be unstable, and mixing may occur. In this study, we

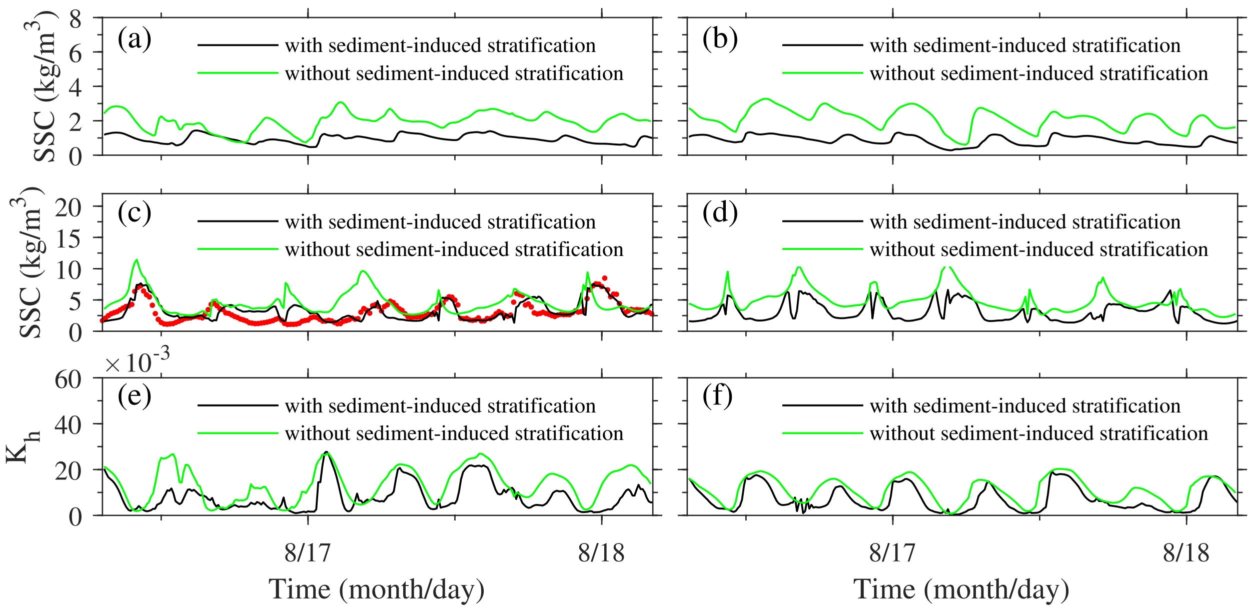

Fig. 11 Temporal variation in surface SSC (**a**, **b**), bottom SSC (**c**, **d**), and vertical eddy diffusivity (**e**, **f**) at sites A (left panel) and B (right panel) in Exp 0 and Exp 1 during the typhoon. Red dots: measured data, same below

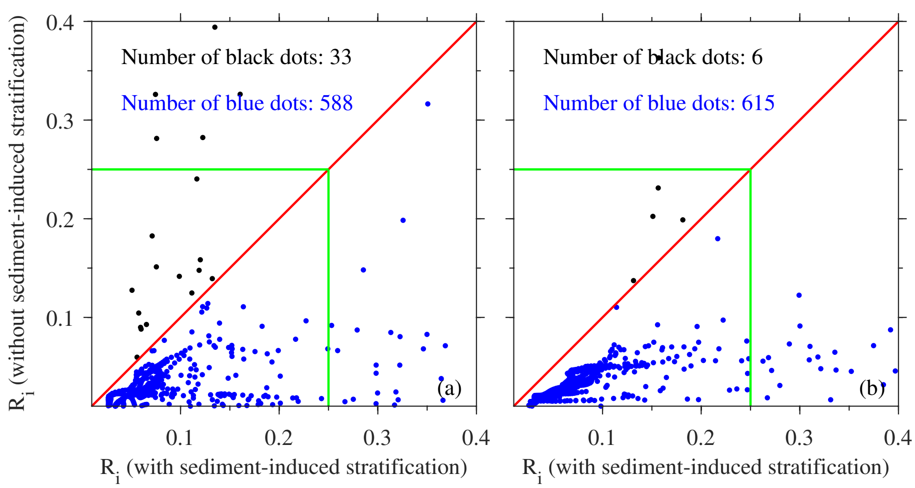

Fig. 12 Comparison of R_i at site A (**a**) and site B (**b**) with and without sediment-induced stratification during the typhoon. The blue dots: R_i at the current moment of Exp 0 is greater than Exp 1; the black dots: the opposite situation; the green line: the threshold of 0.25

calculate the instantaneous value of R_i at different times to indicate the variation in water mixing intensity.

The comparison of R_i between Exp 0 and Exp 1 at sites A and B during the typhoon are shown in Fig. 12. Each point on the graph represents the relative position of R_i with and without sediment-induced stratification at a certain moment. During the typhoon, the R_i in the water column is almost always increasing after considering sediment-induced stratification (the number of blue dots is much greater than the number of black dots). Therefore, the suppression of vertical mixing by sediment-induced stratification during typhoons should not be ignored.

4.2 Effect of waves

First, let's study the difference in the effects of waves on the water column before and during typhoons. The comparison results of Exp 0 and Exp 2 at sites A and B before the typhoon are shown in Fig. 13, taking August 5 to 8, 2018, as an example. Before the typhoon, the average significant wave height at sites A and B in Hangzhou

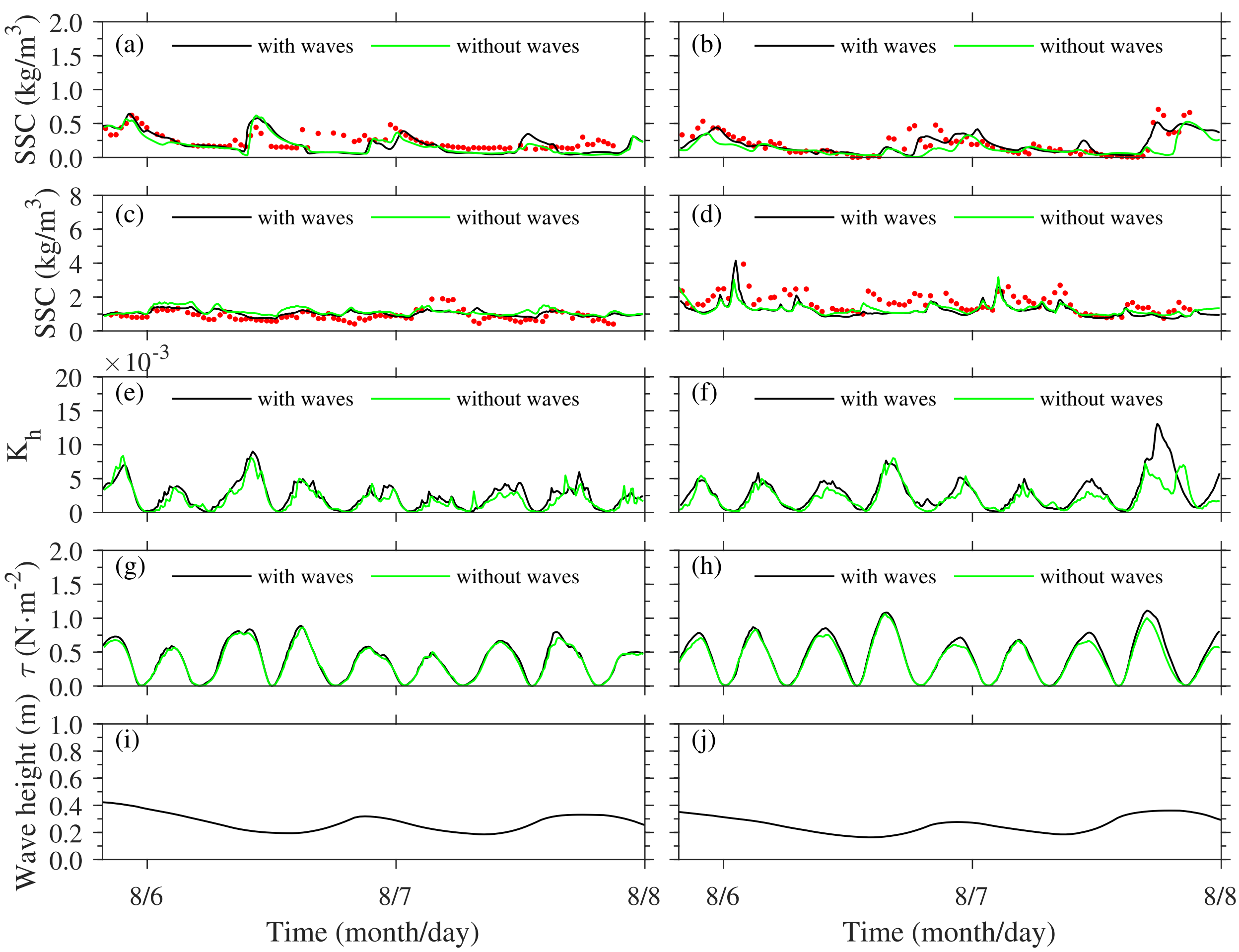

Fig. 13 Temporal variation in surface SSC (**a**, **b**), bottom SSC (**c**, **d**), vertical eddy diffusivity (**e**, **f**), bottom shear stress (**g**, **h**), and significant wave height (**i**, **j**) at sites A (left panel) and B (right panel) in Exp 0 and Exp 2 before the typhoon

Bay were 0.27 m and 0.26 m, respectively. After considering waves before the typhoon, the vertical eddy diffusivity (K_h) at sites A and B increased by 21.1% and 28.2%, respectively, and the simulated surface SSC increased by 11.8% and 44.3%, respectively, indicating that waves significantly increased the vertical mixing in the water column before the typhoon, increasing the surface SSC. After considering waves before the typhoon, the bottom shear stress at sites A and B increased by 5.8% and 10.9%, respectively, while the simulated bottom SSC decreased by 9.3% and 5.7%, respectively, indicating that the wave-induced bottom shear stress before the typhoon is a small amount compared to the tidal-induced bottom shear stress. The upward transport of bottom sediment caused by the enhanced vertical mixing by waves is greater than the increase in sediment resuspension caused by the wave-induced bottom shear stress, thus reducing the bottom SSC. The results show that before typhoons, the effect of waves on vertical mixing is stronger than the effect of wave-induced bottom shear stress on sediment resuspension.

The comparison results of Exp 0 and Exp 2 at sites A and B during the typhoon are shown in Fig. 14. During Typhoon Rumbia, the average significant wave height at sites A and B in Hangzhou Bay were 1.37 m and 1.17 m, respectively, which were significantly higher than those before the typhoon. After considering waves during the typhoon, the simulated surface SSC at sites A and B increased by 4.7% and 1.0%, respectively; the bottom shear stress increased by 41.5% and 52.5%, respectively; the simulated bottom SSC increased by 89.6% and 74.1%, respectively; while K_h decreased by 17.5% and 7.2%, respectively. Compared with before the typhoon, it can be concluded that the effect of waves on the bottom SSC during the typhoon is more significant, while the effect on the surface SSC is less. And the effect of waves at site A is greater than that at site B during the

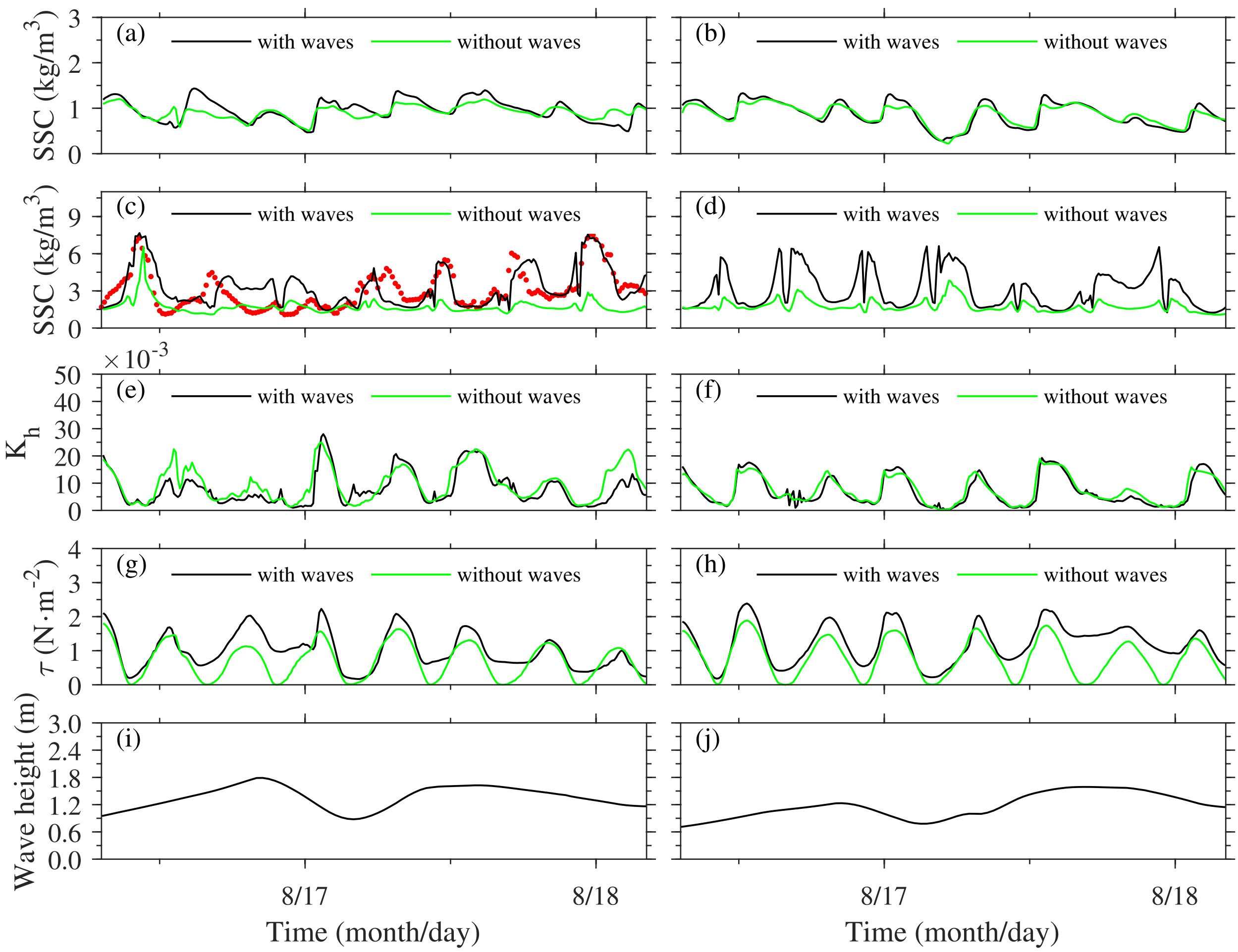

Fig. 14 Temporal variation in surface SSC (**a**, **b**), bottom SSC (**c**, **d**), vertical eddy diffusivity (**e**, **f**), bottom shear stress (**g**, **h**), and significant wave height (**i**, **j**) at sites A (left panel) and B (right panel) in Exp 0 and Exp 2 during the typhoon

typhoon, indicating that the effect of waves near the outside the estuary is more significant.

Theoretically, the waves help to increase the vertical mixing in the water column, which is consistent with the results before typhoons. It is an interesting finding that K_h decreases during typhoons when waves are considered. To show the effect of waves on SSC more graphically, a profile of the SSC at site A is presented, as shown in Fig. 15. Figure 15a shows that the surface and bottom SSC differ greatly during typhoons, especially the bottom SSC gradient, while Fig. 17b shows that the vertical SSC gradient decreases significantly without waves. Section 4.1 concludes that the sediment-induced stratification is highly significant, so it can be deduced that the difference in the vertical SSC caused by waves during typhoons will intensify the sediment-induced stratification effect. On the one hand, waves will directly cause vertical mixing enhancement, and on the other hand, wave-induced bottom shear stress will indirectly cause sediment-induced stratification enhancement to inhibit vertical mixing. The two is a process of mutual cancellation.

According to the above analysis, waves further affect vertical mixing indirectly by changing the vertical SSC gradient. Before typhoons, the direct effect of waves on vertical mixing is stronger than the effect of wave-induced bottom shear stress on the sediment resuspension. While during typhoons, the wave-induced bottom shear stress greatly promotes the sediment resuspension, which indirectly makes the sediment-induced stratification (mainly in the bottom layer) stronger than the direct effect of waves on the vertical mixing in the water column.

The distribution of suspended sediment transport in Hangzhou Bay without waves in Exp 2 is shown in Fig. 16a, c, e. Compared with Fig. 10b, d, f, it can be found that the waves did not significantly change the direction of suspended sediment transport, but significantly affected the amount of suspended sediment transport

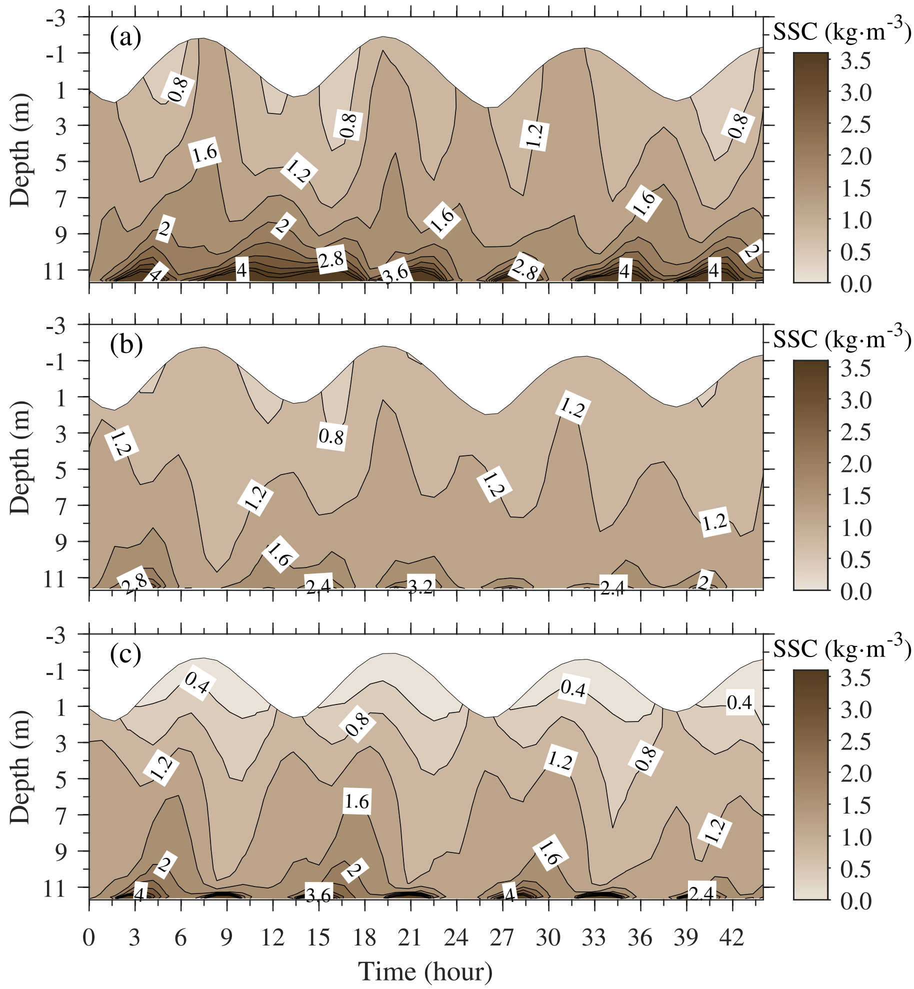

Fig. 15 The vertical profile distributions of SSC at site A during the typhoon. **a** Exp 0; **b** Exp 2; **c** Exp 3

in the bottom and whole layer. The NTSF across the NQ section in Exp 2 decreased by 66.10% compared to Exp 0 (Table 3), which greatly reduced the sediment transport from the Changjiang Estuary to Hangzhou Bay, indicating that waves significantly affected sediment resuspension during typhoons.

4.3 Effect of winds

To further illustrate the effect of strong winds brought by typhoons on the SSC in Hangzhou Bay, Exp 3 is set in this study. The comparison results of Exp 0 and Exp 3 at sites A and B during the typhoon are shown in Fig. 17. After considering winds during the typhoon, K_h at sites A and B increased by 41.4% and 9.6%, respectively; the simulated surface SSC increased by 181.9% and 33.9%, respectively; the simulated bottom SSC increased by 74.2% and 57.0%, respectively, and the bottom shear stress decreased by only 5.4% and 5.1%, respectively. According to the analysis in Sect. 4.2, after waves were removed by Exp 2 during typhoons, the surface SSC decreased very little, while K_h increases instead. When winds were removed in Exp 3, the surface SSC, bottom SSC, and K_h all decreased, while the bottom shear stress increased slightly, indicating that the strong winds brought by typhoons mainly enhanced the vertical mixing, thereby increasing the surface and bottom SSC. From the SSC profile at site A (Fig. 15c), it can be seen that the vertical SSC gradient in Exp 3 is obviously stronger than that in Exp 2, but both weaker than that in Exp 0, especially in the bottom layer. The results further indicated that the effect of waves during typhoons significantly enhanced sediment-induced stratification, while winds had a stronger effect on surface SSC than waves.

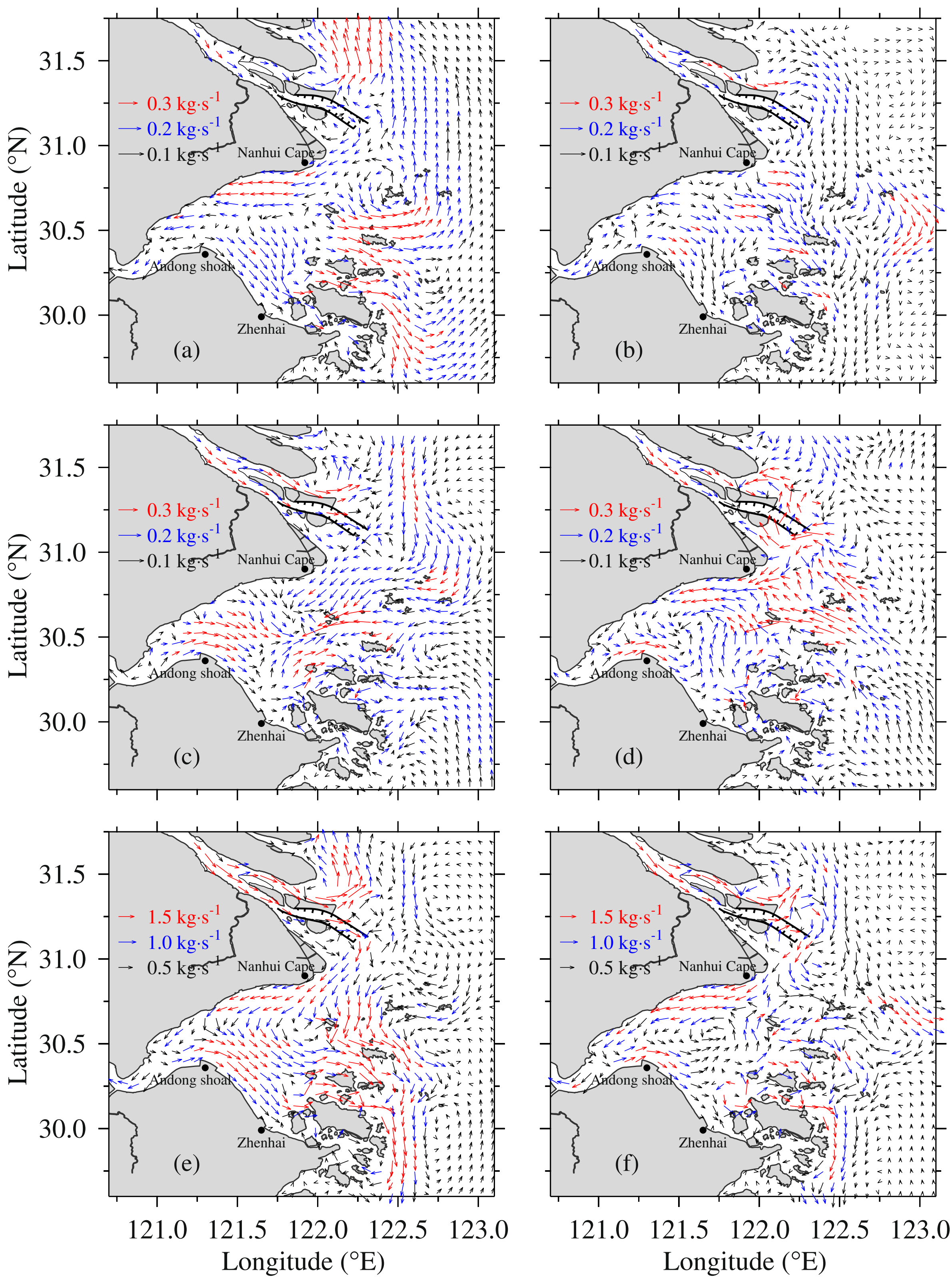

Fig. 16 The distributions of RUSF in the surface layer (**a**, **b**), bottom layer (**c**, **d**), and whole layer (**e**, **f**) in Exp 2 (left panel) and Exp 3 (right panel) during the typhoon

Table 3 NTSF across the NQ section. Negative values indicate sediment flow into Hangzhou Bay, and positive values indicate sediment flow into the Changjiang Estuary

Type	Exp 0	Exp 2	Exp 3
NTSF (10^9 kg)	− 5.34	-1.81	− 2.04
Declining rate (%)	/	66.10	61.80

The distribution of suspended sediment transport in Hangzhou Bay without winds in Exp 3 is shown in Fig. 16b, d, f. Compared with Fig. 10b, d, f, it can be found that strong winds have significantly changed the amount and direction of suspended sediment transport in the surface and bottom layers of the bay, but the characteristics of " north-landward and south-seaward " of the RUSF in the whole layer in Hangzhou Bay are still the same. The NTSF across the NQ section in Exp 3 decreased by 61.80% compared to Exp 0 (Table 3), indicating that the strong winds during typhoons can promote sediment transport from the Changjiang Estuary to Hangzhou Bay.

5 Conclusion

Based on the ECOM-si three dimensional numerical model, a three dimensional suspended sediment numerical model was established to simulate and analyze the effect of typhoons on sediment transport in Hangzhou Bay, in which advection, diffusion, flocculation, settlement, waves, sediment-induced stratification, and other factors were considered. The numerical model can sufficiently reproduce the variation in SSC during typhoons. The transport of water and sediment during Typhoon Rumbia in 2018 was simulated and analyzed. During typhoons, the water and suspended sediment transport in Hangzhou Bay showed a pattern of "north-landward and south-seaward", which made the suspended sediment converge in the central part of the bay. During Typhoon Rumbia, the NTWF and NTSF across the NQ section increased by 18.13% and 265.75%, respectively, compared with those before the typhoon, prompting more suspended sediment to enter Hangzhou Bay.

For high turbidity waters, such as those in Hangzhou Bay, the simulated SSC during typhoons was much more consistent with the observed values after considering the sediment-induced stratification. The suppression of vertical mixing by sediment-induced stratification during typhoons should not be ignored. The wave-induced bottom shear stress during typhoons has a very significant impact on the bottom SSC, which greatly promotes sediment resuspension. The strong winds brought by typhoons

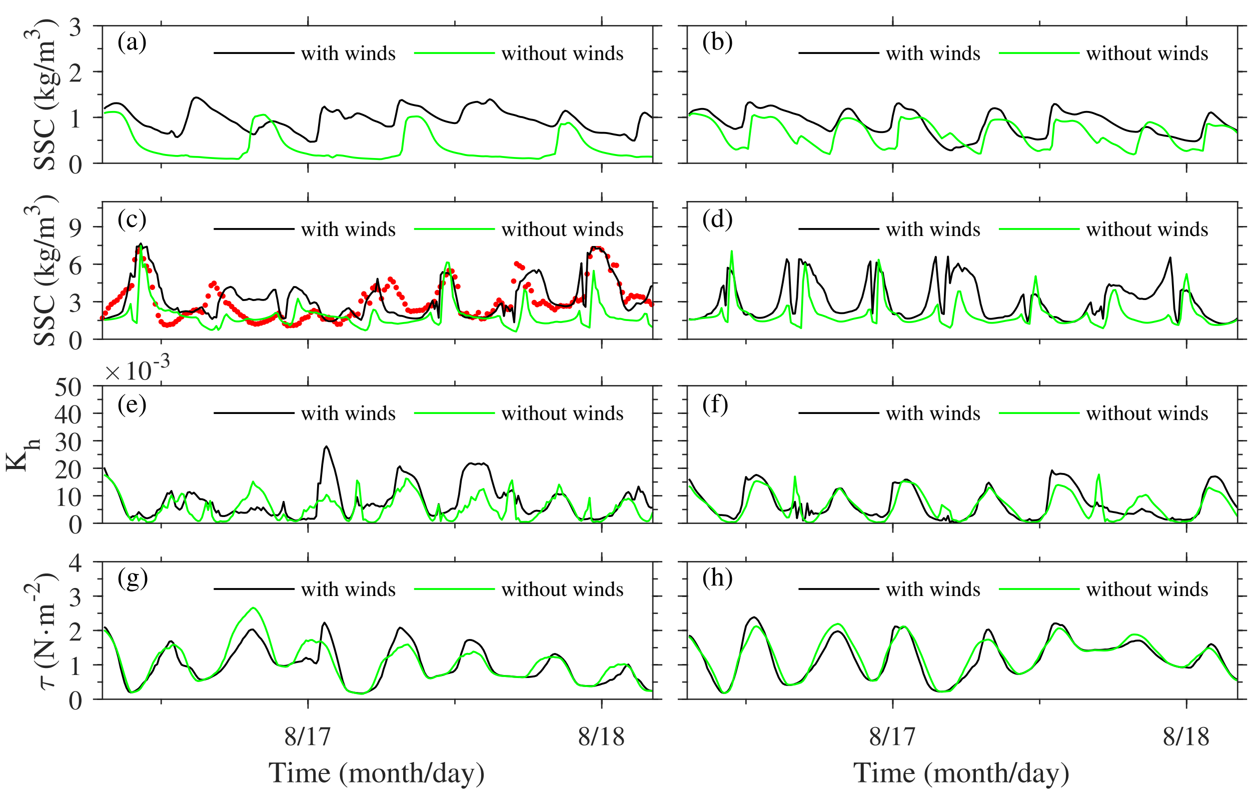

Fig. 17 Temporal variation in surface SSC (**a**, **b**), bottom SSC (**c**, **d**), vertical eddy diffusivity (**e**, **f**), and bottom shear stress (**g**, **h**) at sites A (left panel) and B (right panel) in Exp 0 and Exp 3 during the typhoon

mainly enhanced the vertical mixing, which has a stronger effect on surface SSC than waves. Before typhoons, the direct effect of waves on vertical mixing is stronger than the effect of wave-induced bottom shear stress on the sediment resuspension. While during typhoons, the wave-induced bottom shear stress greatly promotes the sediment resuspension, which indirectly makes the sediment-induced stratification stronger than the direct effect of waves on the vertical mixing.

Abbreviations

SSC	Suspended sediment concentration
NQ section	Section from Nanhui Cape to Qiqu Archipelago
ECOM-si	Estuary, Coast, and Ocean Model with semi-implicit
SWAN	Simulating Waves Nearshore
ADCP	Acoustic Doppler current profiler
OBS	Optical backscatter sensor
Alec	Electromagnetic current meter
ECMWF	European Centre for Medium-Range Weather Forecast
ERA5	ECMWF Reanalysis v5
CC	Correlation coefficient
RMSE	Root mean square error
SS	Skill score
RUWF	Residual unit width water flux
RUSF	Residual unit width sediment flux
NTWF	Net transect water flux
NTSF	Net transect sediment flux

Acknowledgements
We acknowledge the anonymous reviewers for their valuable comments and suggestions.

Authors' contributions
Conceptualization, J.H. and J.Z.; methodology, J.H.; software, J.H. and J.Z.; validation, J.H.; formal analysis, J.H.; investigation, J.H.; resources, J.H. and J.Z.; data curation, J.H.; writing—original draft preparation, J.H.; writing—review and editing, J.Z.; visualization, J.H.; supervision, J.Z.; project administration, J.Z.; funding acquisition, J.Z. All authors have read and agreed to the published version of the manuscript.

Funding
This work was supported by the Science and Technology Commission of Shanghai Municipality (21JC1402500, 22JC1400900).

Availability of data and materials
The frst author, Dr. Ju Huang (huangjuecnu@163.com) can be contacted for access to the data.

Declarations

Ethics approval and consent to participate
Our study is based on open source data and numerical model, so there are no ethical issues.

Consent for publication
Not applicable.

Competing interests
The authors declare no competing interests.

Received: 1 November 2022 Revised: 10 January 2023 Accepted: 23 January 2023
Published online: 06 February 2023

References

Arakawa A, Lamb VR (1977) Computational design of the basic dynamical processes of the UCLA general circulation model. General Circulation Models Atmosphere 17(Supplement C):173–265
Bian C, Jiang W, Song D (2010) Terrigenous transportation to the Okinawa Trough and the influence of typhoons on suspended sediment concentration. Cont Shelf Res 30(10–11):1189–1199. https://doi.org/10.1016/j.csr.2010.03.008
Blumberg AF, Mellor GL (1987) A description of a three-dimensional coastal ocean circulation model. Three-Dimensional Coastal Ocean Models 4:1–16. https://doi.org/10.1029/CO004p0001
Booij N, Ris RC, Holthuijsen LH (1999) A third-generation wave model for coastal regions: 1. Model description and validation. J Geophys Res Oceans 104(C4):7649–7666. https://doi.org/10.1029/98JC02622
Brand A, Lacy JR, Hsu K, Hoover D, Gladding S, Stacey MT. 2010. Wind-enhanced resuspension in the shallow waters of South San Francisco Bay: Mechanisms and potential implications for cohesive sediment transport. J Geophys Res Oceans, 115 (C11). https://doi.org/10.1029/2010JC006172
Casulli V, Cattani E (1994) Stability, accuracy and efficiency of a semi-implicit method for three-dimensional shallow water flow. Computers Mathematics with Applications 27(4):99–112. https://doi.org/10.1016/0898-1221(94)90059-0
Chen CS, Zhu JR, Zheng LY, Ralph E, Budd JW (2004) A non-orthogonal primitive equation coastal ocean circulation model: application to Lake Superior. J Gt Lakes Res 30:41–54. https://doi.org/10.1016/S0380-1330(04)70376-7
Chen Q, Zhu JR, Lyu HH, Pan SQ, Chen SL (2019) Impacts of topography change on saltwater intrusion over the past decade in the Changjiang Estuary. Estuarine, Coastal Shelf Science 231:106469
Du PJ, Ding PX, Hu KL (2010) Simulation of three-dimensional cohesive sediment transport in Hangzhou Bay, China. Acta Oceanologica Sinica 29(2):98–106
Fang HW, Huang L, Wang JY, He GJ, Reible D (2016) Environmental assessment of heavy metal transport and transformation in the Hangzhou Bay, China. J Hazard Mater 302:447–457. https://doi.org/10.1016/j.jhazmat.2015.09.060
Galperin B, Sukoriansky S, Anderson PS (2007) On the critical Richardson number in stably stratified turbulence. Atmospheric Science Letters 8(3):65–69. https://doi.org/10.1002/asl.153
Gong W, Shen J (2009) Response of sediment dynamics in the York River Estuary, USA to tropical cyclone Isabel of 2003. Estuarine Coastal Shelf Science 84(1):61–74. https://doi.org/10.1016/j.ecss.2009.06.004
Grant WD, Madsen OS (1979) Combined wave and current interaction with a rough bottom. J Geophys Res Oceans 84(C4):1797–1808
Grant WD, Madsen OS (1986) The continental-shelf bottom boundary layer. Annu Rev Fluid Mech 18(1):265–305
Green MO, Coco G (2014) Review of wave-driven sediment resuspension and transport in estuaries. Rev Geophys 52(1):77–117. https://doi.org/10.1002/2013RG000437
Hsu T, Elgar S, Guza R (2006) Wave-induced sediment transport and onshore sandbar migration. Coast Eng 53(10):817–824. https://doi.org/10.1016/j.coastaleng.2006.04.003
Huang YG, Yang HF, Yang SL, Wang YP, Dai ZJ, Shi BW, Wu QY (2021) Decadal Decreases of Suspended Sediment Concentrations within the Yangtze River Estuary: A Response to Human Impacts. J Coast Res 37(4):852–863. https://doi.org/10.2112/JCOASTRES-D-20-00035.1
Huang J, Yuan R, Zhu J (2022) Numerical simulation and analysis of water and suspended sediment transport in Hangzhou Bay, China. Journal of Marine Science and Engineering 10(9):1248. https://doi.org/10.3390/jmse10091248
Kantha LH, Clayson CA (1994) An improved mixed layer model for geophysical applications. J Geophys Res Oceans 99(C12):25235–25266. https://doi.org/10.1029/94JC02257
Li M, Yang W, Sun T, Jin YW (2016a) Potential ecological risk of heavy metal contamination in sediments and macrobenthos in coastal wetlands induced by freshwater releases: a case study in the Yellow River Delta. China Mar Pollut Bull 103(1–2):227–239. https://doi.org/10.1016/j.marpolbul.2015.12.014
Li X, Zhu J, Yuan R, Qiu C, Wu H (2016b) Sediment trapping in the Changjiang Estuary: Observations in the North Passage over a spring-neap tidal cycle. Estuarine Coastal Shelf Science 177:8–19. https://doi.org/10.1016/j.ecss.2016.05.004

Li L, Shen F, He Z, Yu Z (2022) Suspended sediment dynamics in macrotidal turbid Hangzhou Bay during Typhoon Chan-hom. Front Earth Sci 10:932149. https://doi.org/10.3389/feart.2022a.932149
Li L, Xu J, Ren Y, Wang XH, Xia YJ (2022) Effects of wave-current interactions on sediment dynamics in Hangzhou Bay during Typhoon Mitag. Front Earth Sci 10:931472. https://doi.org/10.3389/feart.2022b.931472
Liu X, Kuang C, Huang S, Dong W (2022) Modelling morphodynamic responses of a natural embayed beach to Typhoon Lekima encountering different tide types. Anthropocene Coasts 5(1):1–11. https://doi.org/10.1007/s44218-022-00004-4
Lu J, Jiang J, Li A, Ma X (2018) Impact of Typhoon Chan-hom on the marine environment and sediment dynamics on the inner shelf of the East China Sea: In-situ seafloor observations. Mar Geol 406:72–83. https://doi.org/10.1016/j.margeo.2018.09.009
Luo ZF, Zhu JR, Wu H, Li XY (2017) Dynamics of the sediment plume over the Yangtze Bank in the Yellow and East China Seas. J Geophys Res Oceans 122(12):10073–10090. https://doi.org/10.1002/2017JC013215
Lyu HH, Zhu JR (2018) Impact of the bottom drag coefficient on saltwater intrusion in the extremely shallow estuary. J Hydrol 557:838–850. https://doi.org/10.1016/j.jhydrol.2018.01.010
Mellor G, Blumberg A (2004) Wave breaking and ocean surface layer thermal response. J Phys Oceanogr 34(3):693–698. https://doi.org/10.1175/2517.1
Mellor GL, Yamada TJ (1982) Development of a turbulence closure model for geophysical fluid problems. Rev Geophys 20(4):851–875. https://doi.org/10.1029/RG020i004p00851
Miles JW (1961) On the stability of heterogeneous shear flows. J Fluid Mech 10(4):496–508. https://doi.org/10.1017/S0022112061000305
Murphy AH (1988) Skill scores based on the mean square error and their relationships to the correlation coefficient. Mon Weather Rev 116(12):2417–2424. https://doi.org/10.1175/1520-0493(1988)116%3c2417:SSBOTM%3e2.0.CO;2
Palinkas CM, Halka JP, Li M, Sanford LP, Cheng P (2014) Sediment deposition from tropical storms in the upper Chesapeake Bay: Field observations and model simulations. Cont Shelf Res 86:6–16. https://doi.org/10.1016/j.csr.2013.09.012
Qiu C, Zhu JR (2013) Influence of seasonal runoff regulation by the Three Gorges Reservoir on saltwater intrusion in the Changjiang River Estuary. Cont Shelf Res 71:16–26. https://doi.org/10.1016/j.csr.2013.09.024
Ren J, Xu F, He Q, Shen J, Guo L, Xie W, Zhu LJG (2021) The role of a remote tropical cyclone in sediment resuspension over the subaqueous delta front in the Changjiang Estuary. China 377:107564
Richardson LF (1920) The supply of energy from and to atmospheric eddies. Proceedings of the Royal Society of London. Series A Containing Papers of a Mathematical Physical Character 97(686):354–373. https://doi.org/10.1098/rspa.1920.0039
Shen Q, Huang W, Qi, D.J.J.o.W., Port, Coastal, Engineering, O. (2018) Integrated modeling of Typhoon Damrey's effects on sediment resuspension and transport in the north passage of Changjiang Estuary, China. J Waterway Port Coastal Ocean Eng 144(6):04018015
Smagorinsky J (1963) General circulation experiments with the primitive equations: I. The basic experiment. Monthly Weather Review 91(3):99–164. https://doi.org/10.1175/1520-0493(1963)091%3c0099:GCEWTP%3e2.3.CO;2
Syvitski JP, Vorosmarty CJ, Kettner AJ, Green P (2005) Impact of humans on the flux of terrestrial sediment to the global coastal ocean. Science 308(5720):376–380. https://doi.org/10.1126/science.1109454
Syvitski JP, Kettner AJ, Overeem I, Hutton EW, Hannon MT, Brakenridge GR, Day J, Vörösmarty C, Saito Y, Giosan L (2009) Sinking deltas due to human activities. Nat Geosci 2(10):681–686. https://doi.org/10.1038/ngeo629
Terray EA, Drennan WM, Donelan MA (1999) The vertical structure of shear and dissipation in the ocean surface layer. In Proc. Symp. on the Wind-Driven Air–Sea Interface—Electromagnetic and Acoustic Sensing, Wave Dynamics, and Turbulent Fluxes. University of New South Wales, Sydney, pp. 239–245
Warner, J.C., Geyer, W.R., Lerczak, J.A., 2005. Numerical modeling of an estuary: a comprehensive skill assessment. J Geophys Res Oceans, 110(C5). https://doi.org/10.1029/2004JC002691
Wiberg PL, Sherwood CR (2008) Calculating wave-generated bottom orbital velocities from surface-wave parameters. Computers Geosciences 34(10):1243–1262. https://doi.org/10.1016/j.cageo.2008.02.010
Willmott CJ (1981) On the validation of models. Phys Geogr 2(2):184–194. https://doi.org/10.1080/02723646.1981.10642213
Winterwerp JC (2001) Stratification effects by cohesive and noncohesive sediment. J Geophys Res Oceans 106(C10):22559–22574. https://doi.org/10.1029/2000JC000435
Wu H, Zhu JR, Shen J, Wang H. 2011. Tidal modulation on the Changjiang River plume in summer. J Geophys Res Oceans, 116 (C8). https://doi.org/10.1029/2011JC007209
Wu H, Zhu JR (2010) Advection scheme with 3rd high-order spatial interpolation at the middle temporal level and its application to saltwater intrusion in the Changjiang Estuary. Ocean Model 33(1–2):33–51. https://doi.org/10.1016/j.ocemod.2009.12.001
Xie DF, Wang ZB, Gao S, De Vriend HJ (2009) Modeling the tidal channel morphodynamics in a macro-tidal embayment, Hangzhou Bay, China. Continental Shelf Res 29(15):1757–1767
Xie DF, Gao S, Wang ZB, Pan CH (2013) Numerical modeling of tidal currents, sediment transport and morphological evolution in Hangzhou Bay, China. Int J Sediment Res 28(3):316–328. https://doi.org/10.1016/S1001-6279(13)60042-6
Xie X, Li M, Ni W (2018) Roles of wind-driven currents and surface waves in sediment resuspension and transport during a tropical storm. J Geophys Res Oceans 123(11):8638–8654. https://doi.org/10.1029/2018JC014104
Xu T, You X (2017) Numerical simulation of suspended sediment concentration by 3D coupled wave-current model in the Oujiang River Estuary, China. Cont Shelf Res 137:13–24. https://doi.org/10.1016/j.csr.2017.01.021
Zhang G, Chen Y, Cheng W, Zhang H, Gong W (2021) Wave effects on sediment transport and entrapment in a channel-shoal estuary: the Pearl River estuary in the dry winter season. J Geophys Res Oceans 126(4):e2020JC016905. https://doi.org/10.1029/2020JC016905
Zhao X, Wang SS, Pan CH, Mu JB, Li LW, Zhu YZ (2018) Distribution characteristics and ecological risk assessment of nutrients in sediment particles in Hangzhou Bay, China, IOP Conference Series: Earth and Environmental Science. IOP Publishing, Taiwan, p 012079
Zhu CY, van Maren DS, Guo LC, Lin JL, He Q, Wang ZB (2021) Effects of Sediment-Induced Density Gradients on the Estuarine Turbidity Maximum in the Yangtze Estuary. J Geophys Res Oceans 126(5):e2020JC016927. https://doi.org/10.1029/2020JC016927
Zhu JR, Wu H, Li L (2015) Hydrodynamics of the Changjiang Estuary and adjacent seas, Ecological Continuum from the Changjiang (Yangtze River) Watersheds to the East China Sea Continental Margin. Springer International Publishing, Cham, pp. 19–45. https://doi.org/10.1007/978-3-319-16339-0_2